ACS APPLIED MATERIALS & INTERFACES

Research Article

Cite This: ACS Appl. Mater. Interfaces 2019, 11, 46912−46919

www.acsami.org

Nanocomposites Based on Ruthenium Nanoparticles Supported on Cobalt and Nitrogen-Codoped Graphene Nanosheets as Bifunctional Catalysts for Electrochemical Water Splitting

Ting He,[†,‡] Yi Peng,[‡] Qiaoxia Li,[‡,§] Jia En Lu,[‡] Qiming Liu,[‡] Rene Mercado,[‡] Yang Chen,[†] Forrest Nichols,[‡] Yi Zhang,*[,†] and Shaowei Chen*[,‡]

[†]Hunan Provincial Key Laboratory of Chemical Power Sources, College of Chemistry and Chemical Engineering, Central South University, Changsha 410083, China

[‡]Department of Chemistry and Biochemistry, University of California, 1156 High Street, Santa Cruz, California 95064, United States

[§]Shanghai Key Laboratory of Materials Protection and Advanced Materials in Electric Power, College of Environmental and Chemical Engineering, Shanghai University of Electric Power, 2588 Changyang Road, Yangpu District, Shanghai 200090, China

Supporting Information

ABSTRACT: Rational design and engineering of high-efficiency electrocatalysts toward overall water splitting is crucial for the development of hydrogen energy technology. Herein, a facile procedure is described for the preparation of effective bifunctional electrocatalysts for both hydrogen evolution reaction (HER) and oxygen evolution reaction (OER), where ruthenium nanoparticles are supported on graphene nanosheets that are codoped with atomic cobalt and nitrogen by controlled pyrolysis of melamine-functionalized graphene oxide and metal ion precursors. The obtained nanocomposites (CoNG/Ru) exhibit a remarkable electrocatalytic activity toward both HER and OER in alkaline media, with a respective overpotential of only −15 and +350 mV to reach the current density of 10 mA cm^{-2}, which is much better than the monometallic counterparts and relevant catalysts in the literature. With CoNG/Ru as bifunctional catalysts for overall water splitting in a two-electrode system, a low potential of 1.58 V is needed to reach the current density of 10 mA cm^{-2}, which is even better than that with commercial Pt/C and RuO_2 catalysts. This is ascribed to the synergistic interactions between the metal species by metal−metal charge transfer. These results highlight the significance of exploiting the electronic interactions between metal species in carbon-based nanocomposites to develop bifunctional catalysts for electrochemical energy technologies.

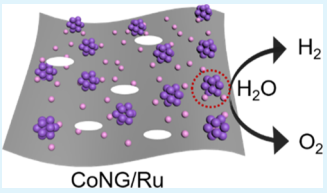

KEYWORDS: *nitrogen-doped graphene, cobalt, ruthenium nanoparticle, bifunctional catalyst, water splitting*

INTRODUCTION

Electrocatalytic water splitting represents an effective, renewable technology for energy conversion and storage, which entails two major reactions, oxygen evolution reaction (OER) at the anode and hydrogen evolution reaction (HER) at the cathode.[1,2] Platinum-based nanoparticles have been the catalysts of choice for HER, while the leading OER catalysts are Ru- and Ir-based oxides.[3] Despite the high electrocatalytic activity of these precious metal-based catalysts, their high costs and low natural abundance have severely hampered the widespread application of the technology. In addition, none of these displays a satisfactory performance toward both HER and OER, which complicates the implementation of the technology and increases the cost of commercialization as the catalysts have to be prepared separately.[4] Therefore, it is of fundamental and technological significance to develop low-cost, high-efficiency bifunctional electrocatalysts toward both HER and OER for overall water splitting.[3−7]

Transition metal/carbon nanocomposites represent a viable candidate,[8,9] by taking advantage of the highly active metal sites, high electrical conductivity of the carbon substrates, synergistic interactions between the metals and the carbon substrate, and ready manipulation of the chemical compositions and structures.[1,10−15] In fact, a wide range of metal/carbon nanocomposites have been developed for water splitting electrocatalysis, such as transition metal alloy/carbon, metal oxide/carbon, metal hydroxide/carbon, metal sulfide/carbon, metal phosphide/carbon, and so forth.[16−21] For instance, the HER activity of ternary FeCoNi alloys encapsulated in graphene can be improved by reducing the content of Ni because of a change of the number of electron transfer from the alloy core to the graphene shell.[17] Nevertheless, currently, most carbon/carbon nanocomposites based on Fe, Co, and Ni exhibit rather high overpotentials for HER in alkaline media (η_{10}, the overpotential needed to reach the current density of 10 mA cm^{-2}, is generally −150 to −200 mV), which severely limits the efficiency of overall water splitting.[4,22,23] Thus, development of high-performance HER catalysts remains a great challenge and is of urgent need. Toward this end, ruthenium has been attracting extensive

Received: September 20, 2019
Accepted: November 22, 2019
Published: November 22, 2019

DOI: 10.1021/acsami.9b17056
ACS Appl. Mater. Interfaces 2019, 11, 46912−46919

attention, as the ruthenium−hydrogen (Ru−H) bond possesses a moderate bond strength similar to that of Pt−H, which is critical for fast HER kinetics.[24] Indeed, ruthenium nanoparticles or even single atoms dispersed in carbon have been found to exhibit remarkable HER electrocatalytic activity, a performance that can even rival that of commercial Pt/C.[25−30] However, these catalysts exhibit only poor OER activity because of low adsorption of oxygen intermediates.[21,31,32] Thus, further structural engineering is needed to render the catalysts active toward OER as well. This can be achieved by the integration of a second metal (e.g., cobalt) into the Ru-based catalysts. Prior studies have shown that Co single atom sites embedded within a N-doped carbon matrix, mostly in the form of CoN_xC_y, display excellent OER activity because of the low barriers for both the oxidation of OH* to O* and desorption of O_2*.[33−35] Thus, integration of Ru and Co species into the carbon nanocomposites may lead to the development of bifunctional electrocatalysts toward both HER and OER. Significantly, metal−metal charge transfer (MMCT) may occur between the two different metal sites, a unique property that can be exploited for the deliberate manipulation of the electronic properties of the materials and hence electrocatalytic performances.

In the present study, a facile procedure was developed to prepare carbon-based nanocomposites, where cobalt was atomically dispersed into N-doped graphene and ruthenium nanoparticles were deposited onto the graphene surface. The obtained nanocomposites exhibited apparent electrocatalytic activity toward both HER and OER. Mechanistically, the HER activity arose from the Ru nanoparticles, and the Co sites were responsible for the OER activity,[33−35] which was aided by MMCT between the two metal components. Remarkably, the electrocatalytic performances toward HER, OER, and overall water splitting were markedly enhanced, as compared to the corresponding monometallic counterparts and commercial catalysts of Pt/C and RuO_2. Results from the present study suggest that structural engineering is an efficient strategy for the rational design and engineering of bifunctional electrocatalysts for overall water splitting.

RESULTS AND DISCUSSION

The synthesis of CoNG/Ru nanocomposites is illustrated in Scheme 1. Experimentally, melamine was dispersed into a graphene oxide (GO) solution under sonication overnight, followed by hydrothermal treatment at 180 °C for 12 h to obtain melamine-functionalized reduced graphene oxide (rGO) nanosheets. The dispersion was then refluxed at 90 °C, into which were added Ru^{2+} and Co^{2+} salts such that the metal ions were adsorbed onto melamine-doped rGO nanosheets by coordination interactions with the N sites of melamine. Subsequent pyrolysis at controlled temperatures (e.g., 700 °C) resulted in the formation of CoNG/Ru nanocomposites where Co was atomically dispersed into the N-doped graphene nanosheets and Ru nanoparticles were deposited onto the graphene surface. In this process, melamine not only served as the N source but also provided the N coordination sites for metal ion complexation to limit aggregation of metal atoms during high-temperature pyrolysis.

Scheme 1. Schematic Illustration of the Preparation of N-Doped Graphene with Ru Nanoparticles and Co Atoms

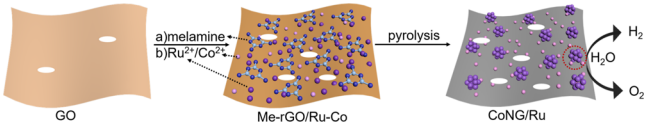

The structures of the nanocomposites were first characterized by transmission electron microscopy (TEM) measurements. From Figures 1a and S1, the control sample prepared without Co(NG/Ru) can be seen to consist of a number of nanoparticles (dia. 1.80 ± 0.44 nm, Figure 1a inset) deposited on thin graphene nanosheets. The CoNG/Ru sample exhibits a similar surface morphology (Figures 1b and S2), except for a small increase of the size of the nanoparticles (2.10 ± 0.33 nm, Figure 1b inset). Notably, for the sample prepared without the addition of ruthenium (CoNG, Figures 1c and S3), only flaky structures were produced and no nanoparticles were found. This suggests that (i) cobalt species were most likely atomically dispersed into the carbon matrix, and (ii) the nanoparticles observed in CoNG/Ru and NG/Ru were derived from ruthenium.[36,37]

Further structural insights of CoNG/Ru were obtained by high-angle annular dark-field scanning TEM (HAADF-STEM) and elemental mapping measurements. From Figure 1d, one can see that N, Ru, and Co elements were indeed successfully integrated into the carbon skeleton. In fact, Ru (Figure 1d_3) can be found to reside only in the area of the nanoparticles in the HAADF-STEM image (highlighted by the red cycles, as compared to the background, pink circles), while the Co element (Figure 1d_2) was evenly distributed across the entire graphene sheets, suggesting that Ru nanoparticles were deposited on the surface of graphene nanosheets that were doped with Co and N. More assertive proofs can be found from higher-resolution elemental mapping as shown in Figure S4. From high-resolution TEM (HRTEM) measurements (Figures 1e,f, S5, and S6), the nanoparticles can be seen to exhibit well-defined lattice fringes, with an interplanar spacing of 2.14 and 2.34 nm, which are consistent with the (002) and (100) facets of hexagonal Ru (PDF 65-7646),[38] whereas the atomic lattices and corresponding diffraction point of the background (Figures 1g and S7) were attributed to the (002) facet of hexagonal graphene (PDF 65-6212).[39]

Consistent results were obtained in the corresponding fast Fourier transform (FFT) diagrams (insets of Figures 1e−g and S7), in good agreement with the X-ray diffraction (XRD) patterns (Figure 2a). In the XRD patterns of NG/Ru and CoNG/Ru, the peak at 2θ = 26.5° can be assigned to the (002) facet of graphene, whereas those at 38.4, 42.2, 44.0, 58.3, 69.4, and 78.4° are due to the (100), (002), (101), (102), (110), and (103) diffractions of hexagonal Ru (PDF 65-7646),[38] confirming the formation of ruthenium nanoparticles in the sample. It is interesting to note that no diffraction feature was observed for the cobalt species, most likely because of the atomic dispersion of Co in CoNG/Ru.[36,37] In fact, for the CoNG sample, the XRD pattern includes only a single sharp peak at 2θ = 26.5°.[39] These observations are in good agreement with results from the TEM measurements (Figure 1). Taken together, these results confirm that the CoNG/Ru nanocomposites are composed of single atomic Co and N-codoped graphene nanosheets embedded with Ru nanoparticles, as depicted in Scheme 1.

The elemental compositions of the nanocomposites were then examined by inductively coupled plasma-optical emission spectrometry (ICP-OES) measurements, and the results are summarized in Table S1. One can see that the total metal

DOI: 10.1021/acsami.9b17056
ACS Appl. Mater. Interfaces 2019, 11, 46912−46919

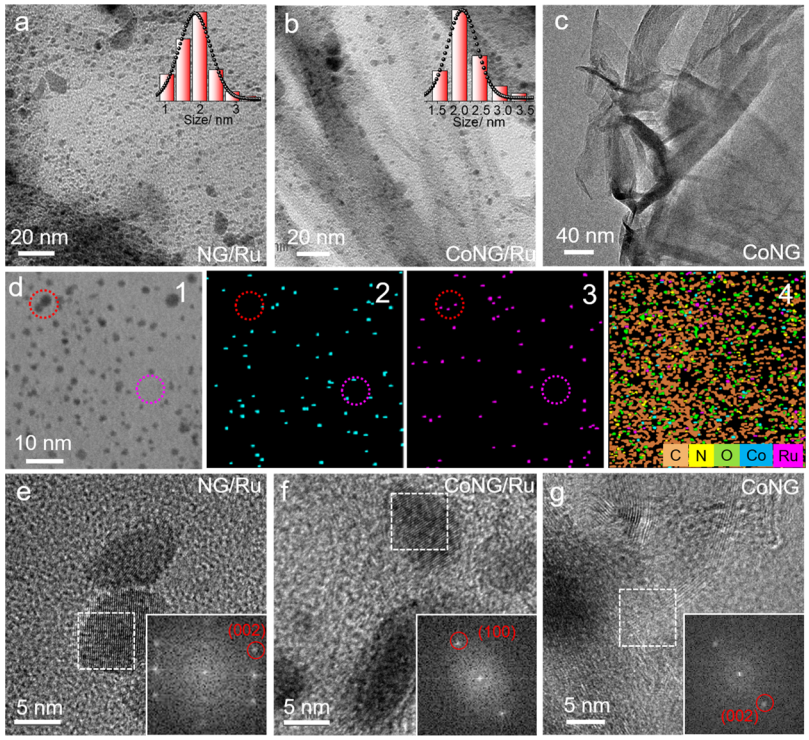

Figure 1. TEM images of (a) NG/Ru and (b) CoNG/Ru. Insets are the corresponding nanoparticle core size histograms. (c) TEM image of CoNG. (d_1) HAADF-STEM image of CoNG/Ru and the corresponding elemental maps of (d_2) Co, (d_3) Ru, and (d_4) all elements. The red and pink cycles are the representative regions for elemental mapping with and without metal nanoparticles, respectively. HRTEM images of (e) NG/Ru, (f) CoNG/Ru, and (g) CoNG. Insets are the corresponding FFT diagrams of the boxed areas in the HRTEM images.

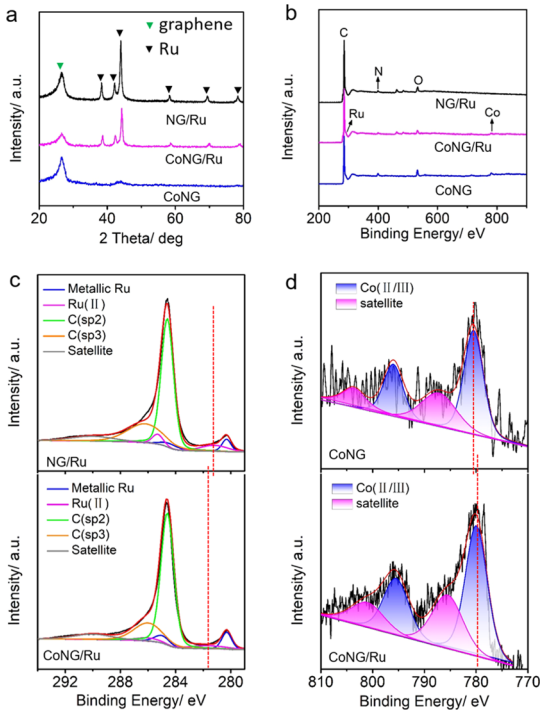

Figure 2. (a) XRD patterns of NG/Ru, CoNG/Ru, and CoNG. (b) XPS survey spectra of NG/Ru, CoNG/Ru, and CoNG. (c) High-resolution XPS scans of the C 1s and Ru 3d electrons in NG/Ru and CoNG/Ru. (d) High-resolution XPS scans of the Co 2p electrons in CoNG and CoNG/Ru. In (c) and (d), the black curves are experimental data and colored curves are deconvolution fits.

content was 4.7 wt% for NG/Ru, 4.6 wt% for CoNG/Ru (including 1.9 wt% Co and 2.7 wt% Ru), and 3.3 wt% for CoNG. X-ray photoelectron spectroscopy (XPS) measurements were then conducted to identify the valence states. The full XPS survey profiles are shown in Figure 2b, where the elements of C/Ru (284 eV), N (400 eV), and Co (780 eV) can be readily identified in CoNG/Ru, while Ru and Co were absent in CoNG and NG/Ru, respectively. The content of each element was also calculated and is shown in Table S2, which was rather consistent with results from ICP-OES measurements (Table S1). High-resolution XPS scans of the C 1s, Ru 3d, and Co electrons are depicted in Figure 2c,d. Deconvolution yields two Ru species, Ru(0) and Ru(II) in the NG/Ru and CoNG/Ru samples (Figure 2c). The former is ascribed to the Ru nanoparticles, while the latter suggests the formation of single Ru atoms coordinated to the nitrogen doping sites (Ru–N).[26] Interestingly, the Ru(II) binding energy for CoNG/Ru (281.4 eV) exhibits a +0.2 eV shift as compared to that of NG/Ru (281.2 eV), while the Ru(0) binding energy (280.3 eV) remained virtually invariant. In the Co 2p scans, the CoNG/Ru sample displayed a pair of peaks at the binding energies of 780.0 and 795.5 eV that are consistent with the Co(II/III) species (the doublets at 785.5 and 801 eV are the satellites),[40] corresponding to a decrease of ca. 0.5 eV as compared to that of CoNG (Figure 2d). This suggests that the incorporation of Co into the nanocomposites led to electron transfer from Ru(II) to Co(II/III). In addition, in comparison with NG/Ru, the doping of Co atoms led to an apparent decrease (1.7 wt%) of Ru(II) (but only a slight decrease of 0.3 wt% of the metallic Ru(0) species). Given that the Ru(II) species stems primarily from Ru atoms coordinated to N dopants, the decrease of Ru–N species in CoNG/Ru is

DOI: 10.1021/acsami.9b17056
ACS Appl. Mater. Interfaces 2019, 11, 46912–46919

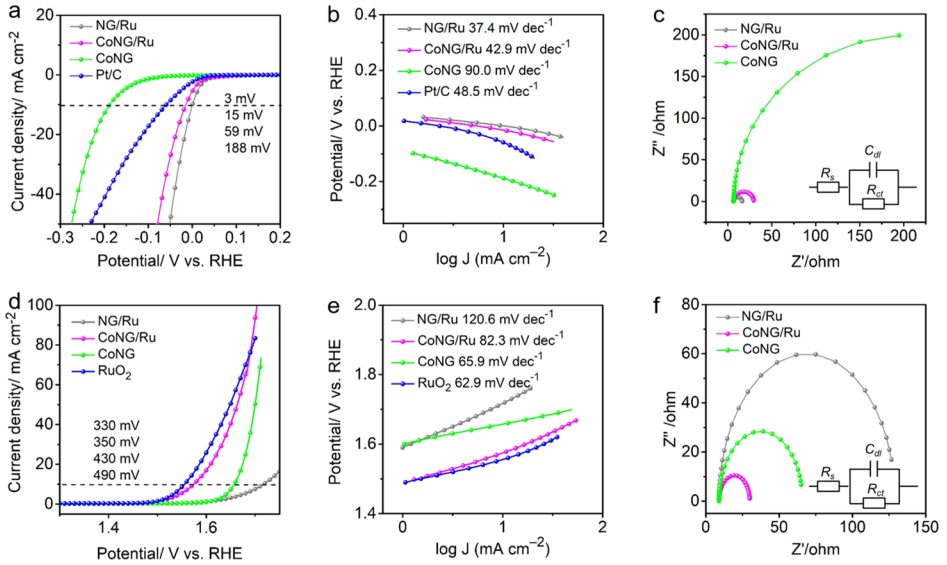

Figure 3. (a) HER polarization curves in 1.0 M KOH of NG/Ru, CoNG/Ru, CoNG, and Pt/C. (b) Tafel plots obtained from the HER polarization curves in (a). (c) Nyquist plots for HER at the overpotential of −15 mV. (d) OER polarization curves in 1.0 M KOH of NG/Ru, CoNG/Ru, CoNG, and Pt/C. (e) Tafel plots obtained from the OER polarization curves in (d). (f) Nyquist plots for OER at the overpotential of +370 mV. Insets of panels (c,f) are the respective equivalent circuits used to fit the data, where R_s, R_{ct}, and C_{dl} stand for the uncompensated resistance, charge transfer resistance, and electrode double-layer capacitance, respectively.

likely due to the competition of Co dopants for the N coordination sites (generating Co−N moieties) (Figure 2d and Table S3). In fact, the fraction of nitrogen in M-N was almost unchanged in CoNG/Ru (0.4 wt%) as compared to that in NG/Ru (0.3 wt%), as manifested in high-resolution scans of the N 1s electrons (Figure S8), which were deconvoluted into four subpeaks corresponding to pyridinic N (398.2 eV), metal-N (399.2 eV), pyrrolic N (400.0 eV), and graphitic N (401.0 eV) (Table S4). As for the C 1s spectra, in addition to the sp^2 and sp^3 carbons, both CoNG/Ru and NG/Ru exhibited a satellite peak at 290.2 eV, which is somewhat stronger in the former than in the latter, suggesting enhanced interaction and graphitization with the introduction of Co dopants (Figure 2c and Table S5),[12,41] in good agreement with the TEM and XRD results presented above. Taken together, the results suggest that the addition of Co dopants led to enhanced graphitization of the nanocomposites, which, along with MMCT between the Ru and Co species, is conducive to enhanced electrocatalytic performance of CoNG/Ru, as compared to NG/Ru and CoNG.

As the Ru and Co species are promising active sites for HER and OER in alkaline media, respectively,[25,26,33,34] the bifunctional electrocatalytic performance was then evaluated by linear sweep voltammetry (LSV) measurements in 1.0 M KOH. From Figure 3a, one can see that the ruthenium-free CoNG exhibits only a low HER activity, needing a high overpotential ($\eta_{10,HER}$) of −188 mV to reach the current density of 10 mA cm^{-2}, a performance similar to leading results of single Co atom catalysts reported in the literature.[42] By contrast, NG/Ru displayed a dramatically reduced $\eta_{10,HER}$ of only −3 mV, signifying the high HER activity of Ru species—note that decreasing the initial Ru feed by half led to only a slight increase of $\eta_{10,HER}$ to −24 mV (Figure S9), suggesting a saturated ruthenium loading in the NG/Ru sample.[31,43,44] For CoNG/Ru, which entails both Co species and Ru nanoparticles, $\eta_{10,HER}$ was also very low at −15 mV, which is 44 mV lower than that of commercial Pt/C (−59 mV). The slightly higher $\eta_{10,HER}$ of CoNG/Ru (−15 mV) than that of NG/Ru (−3 mV) can be ascribed to the lower Ru content in CoNG/Ru (2.7 wt%) than in NG/Ru (4.7 wt%) (Table S1). In fact, at the same content of Ru (2.7 wt%), CoNG/Ru clearly outperformed NG/Ru in HER (Figure S10).

Further mechanistic analysis of the catalytic reaction kinetics was carried out with the Tafel plots. The Tafel slope of CoNG/Ru is estimated to be 42.9 mV dec^{-1}, which is slightly higher than that of NG/Ru (37.4 mV dec^{-1}) but lower than those of Pt/C (48.5 mV dec^{-1}) and CoNG (90.0 mV dec^{-1}) (Figure 3b). This suggests favorable HER kinetics on NG/Ru and CoNG/Ru.[25,45]

Remarkably, the CoNG/Ru nanocomposites also exhibited apparent electrocatalytic activity toward OER. As displayed in Figure 3d, NG/Ru requires a high overpotential ($\eta_{10,OER}$ = +490 mV) to reach the current density of 10 mA cm^{-2}, but CoNG possesses a much better activity with a lower $\eta_{10,OER}$ of +430 mV. This suggests that in CoNG/Ru, the Co sites are more active than the Ru sites toward OER.[33−35] Interestingly, the combination of these two metal sites endows CoNG/Ru an even lower overpotential of $\eta_{10,OER}$ = +350 mV, which is comparable to that of commercial RuO_2 (+330 mV). The obvious enhancement is most likely due to the synergistic interactions between the two metal centers in the CoNG/Ru nanocomposites, as manifested by the MMCT effects observed in XPS measurements (Figure 2).

This synergistic effect can also be manifested by the observation that the OER performance of CoNG/Ru varied with the Co content, and the sample presented above was prepared at the optimal Ru to Co molar feed ratio of 1:0.25 (Figure S11). Additionally, the small Tafel slope of 82.3 mV dec^{-1} further attests the faster reaction kinetics of OER on CoNG/Ru electrocatalysts (Figure 3e).

Electrochemical impedance spectroscopy measurements were then carried out to examine the charge-transfer resistance (R_{ct}) involved in both HER and OER. Figure 3c depicts the Nyquist plots for HER at the overpotential of −15 mV, where

DOI: 10.1021/acsami.9b17056
ACS Appl. Mater. Interfaces 2019, 11, 46912−46919

R_{ct} was estimated to be 23.0 Ω for CoNG/Ru, 9.8 Ω for NG/Ru, and 438.1 Ω for CoNG. Likewise, Figure 3f shows the Nyquist plots for OER at the overpotential of +370 mV, where R_{ct} was estimated to be 21.0, 120.0, and 56.9 Ω, respectively. These results highlight the low charge-transfer resistance of CoNG/Ru in both HER and OER, coinciding with the remarkable electrocatalytic activity. The electrochemical double-layer capacitance (C_{dl}) was then quantitatively assessed to compare the electrochemical surface area of the samples. On the basis of the cyclic voltammograms acquired at the scan rates of 10−50 mV s^{-1}, C_{dl} was estimated to be 12.1 mF cm^{-2} for CoNG/Ru, 9.2 mF cm^{-2} for NG/Ru, and 5.0 mF s^{-1} for CoNG, suggesting enhanced exposure of the electrochemical active sites of the dual-metal catalyst as compared to the monometallic counterparts in the series (Figure S12). Table S6 lists the potential difference (ΔE_{10}) between HER and OER at the current density of 10 mA cm^{-2} ($\Delta E_{10} = E_{10,OER} - E_{10,HER}$) for NG/Ru, CoNG/Ru, CoNG, and Pt/C//RuO_2. The dual-metal catalysts (CoNG/Ru) can be seen to display a ΔE_{10} of only 1.595 V, much lower than 1.723 V for NG/Ru and 1.848 V for CoNG, and even lower than that (1.619 V) for Pt/C and RuO_2.

With such a remarkable bifunctional performance, the CoNG/Ru nanocomposite was then used as both the anode and cathode catalysts for water splitting in a two-electrode setup, and the performance was compared to that using commercial RuO_2 and Pt/C as the anode and cathode catalysts, respectively. Here, Ni foam was utilized as the current collectors (see Experimental Section for more details). Figure 4a shows the LSV of water electrolysis on the as-

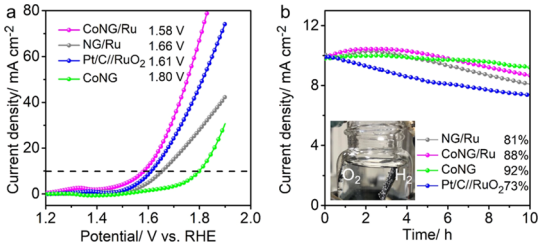

Figure 4. (a) LSV curves of overall water splitting using the catalysts (CoNG/Ru, NG/Ru, Pt/C//RuO_2, and CoNG) as both the anode and cathode at the potential scan rate of 10 mV s^{-1} in 1.0 M KOH. (b) Chronoamperometric curves at the applied potential of 1.58 V for CoNG/Ru, 1.66 V for NG/Ru, 1.80 V for CoNG, and 1.61 V for Pt/C//RuO_2. Inset is a photograph of water splitting by using CoNG/Ru as the bifunctional catalysts.

assembled CoNG/Ru, NG/Ru, and Pt/C//RuO_2 electrodes in a 1.0 M KOH electrolyte solution. The CoNG/Ru cell can be seen to exhibit a high activity, reaching a water-splitting current density of 10 mA cm^{-2} at the applied potential of only 1.58 V, which is superior to those with NG/Ru (1.66 V), CoNG (1.80 V), and even commercial Pt/C//RuO_2 (1.61 V).[46] This is also superior/comparable to leading results reported recently (Table S7).[16,22,47−49] In addition, the long-term stability of CoNG/Ru for overall water splitting was evaluated through a chronoamperometric test.[49] At the cell voltage of 1.58 V, one can see that a large number of oxygen and hydrogen bubbles were produced on the anode and cathode surfaces (Figure 4b inset). After 10 h of continuous electrolysis at 10 mA cm^{-2}, the CoNG/Ru cell retained 88% of the initial current density, in contrast to 81% for NG/Ru, 92% for CoNG, and 73% for Pt/C//RuO_2, suggesting a remarkable stability of CoNG/Ru. Such a high activity and excellent long-term stability confirm that the CoNG/Ru nanocomposites can be exploited as viable bifunctional electrocatalysts for overall water splitting.

To examine the structural integrity of CoNG/Ru during the durability tests, the catalysts were collected from the electrode surfaces after the above-mentioned water splitting operation and analyzed by a range of microscopic and spectroscopic measurements. First of all, in XRD (Figure S13) and XPS (Figure S14) measurements, the results of CoNG/Ru from both the anode and cathode are consistent with those of the as-prepared sample (Figure 2). Nevertheless, TEM measurements (Figure S15) showed a marked increase of the nanoparticle size to 10 ± 5 nm in diameter, as compared to the as-produced sample (Figure 1). Such nanoparticle aggregation is most likely responsible for the attenuation of the catalytic performance (Figure 4b).

CONCLUSIONS

In this study, a facile procedure was developed to prepare CoNG/Ru nanocomposites where ruthenium nanoparticles were deposited on Co and N-codoped graphene nanosheets by controlled pyrolysis of melamine-functionalized GO nanosheets and metal ion precursors. The as-prepared CoNG/Ru nanocomposites exhibited an excellent bifunctional electrocatalytic activity toward both HER and OER, with an overpotential of −15 mV in the former and +350 mV in the latter to reach the current density of 10 mA cm^{-2}, which is much better than those of the monometallic counterparts and relevant catalysts based on transition metal-doped carbons reported in the literature. With CoNG/Ru as the bifunctional electrode catalysts for water splitting in a two-electrode cell, the performance was even better than that with commercial Pt/C and RuO_2 catalysts. The enhanced performance was attributed to the synergistic interactions between the different metal sites, as manifested in MMCT between the Ru and Co species. Results from the study demonstrate the significance of manipulating the electronic structures of transition metal sites in carbon nanocomposites in the development of bifunctional catalysts for electrochemical energy technologies.

EXPERIMENTAL SECTION

Reagents. Graphite powders (Spectrum Chemicals), sodium nitrate ($NaNO_3$, 99%, Acros), sulfuric acid (H_2SO_4, 98%, Fisher Scientific), potassium permanganate ($KMnO_4$, 99%, Fisher Scientific), hydrogen peroxide (H_2O_2, 30%, Fisher Scientific), hydrochloric acid (HCl, 37%, Fisher Scientific), melamine (99%, Acros), ruthenium-(III) chloride ($RuCl_3$, 35−40% Ru, Acros), cobalt(II) chloride ($CoCl_2$, 98%, Fisher Scientific), and potassium hydroxide (KOH, Fisher Scientific) were all used as received. Water was supplied by a Barnstead Nanopure water system (18.3 MΩ cm).

Sample Preparation. GO nanosheets were prepared by following the Hummers' method,[28,50,51] and underwent further chemical functionalization. In brief, 60 mg of GO, 120 mg of melamine, and 30 mL of H_2O were added into a 100 mL flask and mixed under sonication overnight before being loaded into a Teflon-lined autoclave for hydrothermal treatment at 180 °C for 12 h, affording N-doped rGO. The dispersion was transferred to a flask, into which were added 13.4 mg of $RuCl_3$ and 3.8 mg of $CoCl_2$. The flask was then heated in an oil bath at 90 °C for 4.5 h to prepare rGO−Ru−Co, which was obtained by centrifugation at 6000 rpm for 5 min, rinsed with H_2O, and dried at 60 °C in a vacuum oven overnight. The rGO-Ru-Co was then heated at 700 °C for 3 h in a nitrogen atmosphere at the nitrogen flow rate of 150 mL min^{-1}. The resulting sample was denoted as CoNG/Ru.

DOI: 10.1021/acsami.9b17056
ACS Appl. Mater. Interfaces 2019, 11, 46912−46919

Two control samples were synthesized in the same fashion, one without the addition of $RuCl_3$ and the other without $CoCl_2$. The final products were denoted as CoNG and NG/Ru, respectively.

Characterization. TEM measurements were conducted with a Philips CM300 operated at 300 kV. XRD studies were carried out with a Rigaku Americas Miniflex Plus powder diffractometer, and XPS spectra were acquired with a PHI 5400/XPS instrument. ICP-OES studies were performed with a PerkinElmer Optima instrument.

Electrochemistry. Electrochemical tests were carried out in a three-electrode electrochemical cell with a graphite rod as the counter electrode and a Ag/AgCl (1 M KCl) electrode as the reference electrode. The Ag/AgCl electrode was calibrated against a reversible hydrogen electrode (RHE), and all potentials in the present study were referenced to this RHE. To prepare a catalyst ink, 2 mg of the catalysts obtained above was dispersed in 475 μL of ethanol and 25 μL of a Nafion solution (5%) under sonication for 3 h to form a homogeneous dispersion (4 mg mL^{-1}). For HER and OER measurements, the catalyst ink was drop-cast onto a cleaned glassy carbon electrode (as the working electrode) at the catalyst loading of 400 μg cm^{-2} for CoNG/Ru, NG/Ru, and CoNG and 100 μg cm^{-2} for Pt/C and RuO_2.

For overall water splitting, the as-prepared catalysts were used as both the anode and cathode electrodes, and the tests were conducted in a two-electrode configuration. The electrode was composed of two layers, including a Ni foam and a catalyst layer. The Ni foam was subjected to sonication treatment in 0.1 M HCl, H_2O and ethanol, consecutively, and vacuum-dried at 60 °C for 5 h. The catalyst layer was prepared by mixing the CoNG/Ru catalyst, carbon black (as a conductive agent), and polytetrafluoroethylene emulsion (PTFE, 60 wt%, as a binder) at the mass ratio of 12:10:10. Because of the difference in the metal content, the mass loading was 4 mg cm^{-2} for CoNG/Ru (about 5 wt% metal content), 1 mg cm^{-2} for Pt/C (20 wt % metal content), and 1 mg cm^{-2} for RuO_2. The total thickness of the cathode was ca. 0.4 mm after compression with a manual tablet machine and vacuum-drying at 60 °C for 4 h..

■ ASSOCIATED CONTENT

Supporting Information

The Supporting Information is available free of charge at https://pubs.acs.org/doi/10.1021/acsami.9b17056.

Elemental compositions by XPS and ICP-OES analyses; comparison of electrocatalytic performance with the literature results; and additional experimental data (PDF)

■ AUTHOR INFORMATION

Corresponding Authors

*E-mail: yzhangcsu@csu.edu.cn (Y.Z.).
*E-mail: shaowei@ucsc.edu (S.C.).

ORCID

Yi Zhang: 0000-0002-8452-9694
Shaowei Chen: 0000-0002-3668-8551

Author Contributions

The manuscript was written through contributions of all authors. All authors have given approval to the final version of the manuscript.

Notes

The authors declare no competing financial interest.

■ ACKNOWLEDGMENTS

S.C. acknowledged support from the National Science Foundation (CHE-1710408 and CHE-1900235). Y.Z. acknowledged support from the National Natural Science Foundation of China (21972169, 21773311, and 21473257) and Hunan Provincial Science and Technology Plan Project (2017TP1001). T.H. is supported by a research fellowship from the China Scholarships Council (201806370027). TEM and XPS work was carried out at the National Center for Electron Microscopy and Molecular Foundry, Lawrence Berkeley National Laboratory, which is supported by the US Department of Energy, as part of a user project.

■ REFERENCES

(1) Chen, S.; Qiao, S.-Z. Hierarchically Porous Nitrogen-Doped Graphene–$NiCo_2O_4$ Hybrid Paper as an Advanced Electrocatalytic Water-Splitting Material. *ACS Nano* **2013**, *7*, 10190–10196.

(2) Wu, Z.; Wang, Z.; Geng, F. Radially Aligned Hierarchical Nickel/Nickel–Iron (Oxy)hydroxide Nanotubes for Efficient Electrocatalytic Water Splitting. *ACS Appl. Mater. Interfaces* **2018**, *10*, 8585–8593.

(3) Pi, Y.; Shao, Q.; Wang, P.; Guo, J.; Huang, X. General Formation of Monodisperse IrM (M = Ni, Co, Fe) Bimetallic Nanoclusters as Bifunctional Electrocatalysts for Acidic Overall Water Splitting. *Adv. Funct. Mater.* **2017**, *27*, 1700886.

(4) Zhong, H.-X.; Wang, J.; Zhang, Q.; Meng, F.; Bao, D.; Liu, T.; Yang, X.-Y.; Chang, Z.-W.; Yan, J.-M.; Zhang, X.-B. In Situ Coupling FeM (M = Ni, Co) with Nitrogen-Doped Porous Carbon toward Highly Efficient Trifunctional Electrocatalyst for Overall Water Splitting and Rechargeable Zn–Air Battery. *Adv. Sustainable Syst.* **2017**, *1*, 1700020.

(5) Liu, W.; Du, K.; Liu, L.; Zhang, J.; Zhu, Z.; Shao, Y.; Li, M. One-Step Electroreductively Deposited Iron-Cobalt Composite Films as Efficient Bifunctional Electrocatalysts for Overall Water Splitting. *Nano Energy* **2017**, *38*, 576–584.

(6) Zhang, P.; Lu, X. F.; Nai, J.; Zang, S.-Q.; Lou, X. W. Construction of Hierarchical Co–Fe Oxyphosphide Microtubes for Electrocatalytic Overall Water Splitting. *Adv. Sci.* **2019**, *6*, 1900576.

(7) Wang, Y.; Yan, D.; El Hankari, S.; Zou, Y.; Wang, S. Recent Progress on Layered Double Hydroxides and Their Derivatives for Electrocatalytic Water Splitting. *Adv. Sci.* **2018**, *5*, 1800064.

(8) He, T.; Wang, X.; Wu, H.; Xue, H.; Xue, P.; Ma, J.; Tan, M.; He, S.; Shen, R.; Yi, L.; Zhang, Y.; Xiang, J. In situ Fabrication of Defective CoNx Single Clusters on Reduced Graphene Oxide Sheets with Excellent Electrocatalytic Activity for Oxygen Reduction. *ACS Appl. Mater. Interfaces* **2017**, *9*, 22490–22501.

(9) Tan, M.; He, T.; Liu, J.; Wu, H.; Li, Q.; Zheng, J.; Wang, Y.; Sun, Z.; Wang, S.; Zhang, Y. Supramolecular Bimetallogels: a Nanofiber Network for Bimetal/Nitrogen Co-doped Carbon Electrocatalysts. *J. Mater. Chem. A* **2018**, *6*, 8227–8232.

(10) Peng, Y.; Lu, B.; Chen, S. Carbon-Supported Single Atom Catalysts for Electrochemical Energy Conversion and Storage. *Adv. Mater.* **2018**, *30*, 1801995.

(11) Peng, Y.; Chen, S. Electrocatalysts Based on Metal@Carbon Core@Shell Nanocomposites: An Overview. *Green Energy Environ.* **2018**, *3*, 335–351.

(12) Kibsgaard, J.; Hellstern, T. R.; Choi, S.-J.; Reinecke, B. N.; Jaramillo, T. F. Mesoporous Ruthenium/Ruthenium Oxide Thin Films: Active Electrocatalysts for the Oxygen Evolution Reaction. *ChemElectroChem* **2017**, *4*, 2480–2485.

(13) Jia, Y.; Zhang, L.; Gao, G.; Chen, H.; Wang, B.; Zhou, J.; Soo, M. T.; Hong, M.; Yan, X.; Qian, G.; Zou, J.; Du, A.; Yao, X. A Heterostructure Coupling of Exfoliated Ni–Fe Hydroxide Nanosheet and Defective Graphene as a Bifunctional Electrocatalyst for Overall Water Splitting. *Adv. Mater.* **2017**, *29*, 1700017.

(14) Pan, Y.; Sun, K.; Liu, S.; Cao, X.; Wu, K.; Cheong, W.-C.; Chen, Z.; Wang, Y.; Li, Y.; Liu, Y.; Wang, D.; Peng, Q.; Chen, C.; Li, Y. Core–Shell ZIF-8@ZIF-67-Derived CoP Nanoparticle-Embedded N-Doped Carbon Nanotube Hollow Polyhedron for Efficient Overall Water Splitting. *J. Am. Chem. Soc.* **2018**, *140*, 2610–2618.

(15) Chen, Y.-Z.; Wang, C.; Wu, Z.-Y.; Xiong, Y.; Xu, Q.; Yu, S.-H.; Jiang, H.-L. From Bimetallic Metal-Organic Framework to Porous Carbon: High Surface Area and Multicomponent Active Dopants for Excellent Electrocatalysis. *Adv. Mater.* **2015**, *27*, 5010–5016.

DOI: 10.1021/acsami.9b17056
ACS Appl. Mater. Interfaces 2019, 11, 46912–46919

(16) Ding, J.; Shao, Q.; Feng, Y.; Huang, X. Ruthenium-Nickel Sandwiched Nanoplates for Efficient Water Splitting Electrocatalysis. *Nano Energy* **2018**, *47*, 1−7.
(17) Yang, Y.; Lin, Z.; Gao, S.; Su, J.; Lun, Z.; Xia, G.; Chen, J.; Zhang, R.; Chen, Q. Tuning Electronic Structures of Nonprecious Ternary Alloys Encapsulated in Graphene Layers for Optimizing Overall Water Splitting Activity. *ACS Catal.* **2017**, *7*, 469−479.
(18) Zhu, C.; Fu, S.; Du, D.; Lin, Y. Facilely Tuning Porous NiCo2O4 Nanosheets with Metal Valence-State Alteration and Abundant Oxygen Vacancies as Robust Electrocatalysts Towards Water Splitting. *Chem.—Eur. J.* **2016**, *22*, 4000−4007.
(19) Feng, L.-L.; Yu, G.; Wu, Y.; Li, G.-D.; Li, H.; Sun, Y.; Asefa, T.; Chen, W.; Zou, X. High-Index Faceted Ni_3S_2 Nanosheet Arrays as Highly Active and Ultrastable Electrocatalysts for Water Splitting. *J. Am. Chem. Soc.* **2015**, *137*, 14023−14026.
(20) Li, Y.; Zhao, C. Enhancing Water Oxidation Catalysis on a Synergistic Phosphorylated NiFe Hydroxide by Adjusting Catalyst Wettability. *ACS Catal.* **2017**, *7*, 2535−2541.
(21) Hu, Q.; Li, G.; Han, Z.; Wang, Z.; Huang, X.; Yang, H.; Zhang, Q.; Liu, J.; He, C. Recent Progress in the Hybrids of Transition Metals/Carbon for Electrochemical Water Splitting. *J. Mater. Chem. A* **2019**, *7*, 14380−14390.
(22) Zhang, Y.; Shao, Q.; Long, S.; Huang, X. Cobalt-Molybdenum Nanosheet Arrays as Highly Efficient and Stable Earth-Abundant Electrocatalysts for Overall Water Splitting. *Nano Energy* **2018**, *45*, 448−455.
(23) Bayatsarmadi, B.; Zheng, Y.; Russo, V.; Ge, L.; Casari, C. S.; Qiao, S.-Z. Highly Active Nickel−Cobalt/Nanocarbon Thin Films as Efficient Water Splitting Electrodes. *Nanoscale* **2016**, *8*, 18507−18515.
(24) Mahmood, J.; Li, F.; Jung, S.-M.; Okyay, M. S.; Ahmad, I.; Kim, S.-J.; Park, N.; Jeong, H. Y.; Baek, J.-B. An Efficient and pH-Universal Ruthenium-Based Catalyst for the Hydrogen Evolution Reaction. *Nat. Nanotechnol.* **2017**, *12*, 441−446.
(25) Chen, C.-H.; Wu, D.; Li, Z.; Zhang, R.; Kuai, C.-G.; Zhao, X.-R.; Dong, C.-K.; Qiao, S.-Z.; Liu, H.; Du, X.-W. Ruthenium-Based Single-Atom Alloy with High Electrocatalytic Activity for Hydrogen Evolution. *Adv. Energy Mater.* **2019**, *9*, 1803913.
(26) Lu, B.; Guo, L.; Wu, F.; Peng, Y.; Lu, J. E.; Smart, T. J.; Wang, N.; Finfrock, Y. Z.; Morris, D.; Zhang, P.; Li, N.; Gao, P.; Ping, Y.; Chen, S. Ruthenium Atomically Dispersed in Carbon Outperforms Platinum toward Hydrogen Evolution in Alkaline Media. *Nat. Commun.* **2019**, *10*, 631−642.
(27) Peng, Y.; Lu, B.; Chen, L.; Wang, N.; Lu, J. E.; Ping, Y.; Chen, S. Hydrogen Evolution Reaction Catalyzed by Ruthenium Ion-Complexed Graphitic Carbon Nitride Nanosheets. *J. Mater. Chem. A* **2017**, *5*, 18261−18269.
(28) Peng, Y.; Pan, W.; Wang, N.; Lu, J.-E.; Chen, S. Ruthenium Ion-Complexed Graphitic Carbon Nitride Nanosheets Supported on Reduced Graphene Oxide as High-Performance Catalysts for Electrochemical Hydrogen Evolution. *ChemSusChem* **2018**, *11*, 130−136.
(29) Xu, Y.; Yin, S.; Li, C.; Deng, K.; Xue, H.; Li, X.; Wang, H.; Wang, L. Low-Ruthenium-Content NiRu Nanoalloys Encapsulated in Nitrogen-Doped Carbon as Highly Efficient and pH-Universal Electrocatalysts for the Hydrogen Evolution Reaction. *J. Mater. Chem. A* **2018**, *6*, 1376−1381.
(30) Xu, J.; Liu, T.; Li, J.; Li, B.; Liu, Y.; Zhang, B.; Xiong, D.; Amorim, I.; Li, W.; Liu, L. Boosting the Hydrogen Evolution Performance of Ruthenium Clusters through Synergistic Coupling with Cobalt Phosphide. *Energy Environ. Sci.* **2018**, *11*, 1819−1827.
(31) Song, Q.; Qiao, X.; Liu, L.; Xue, Z.; Huang, C.; Wang, T. Ruthenium@N-doped Graphite Carbon Derived from Carbon Foam for Efficient Hydrogen Evolution Reaction. *Chem. Commun.* **2019**, *55*, 965−968.
(32) Hwang, H.; Kwon, T.; Kim, H. Y.; Park, J.; Oh, A.; Kim, B.; Baik, H.; Joo, S. H.; Lee, K. Ni@Ru and NiCo@Ru Core−Shell Hexagonal Nanosandwiches with a Compositionally Tunable Core and a Regioselectively Grown Shell. *Small* **2018**, *14*, 1702353.
(33) Liu, X.; Wang, L.; Yu, P.; Tian, C.; Sun, F.; Ma, J.; Li, W.; Fu, H. A Stable Bifunctional Catalyst for Rechargeable Zinc−Air Batteries: Iron−Cobalt Nanoparticles Embedded in a Nitrogen-Doped 3D Carbon Matrix. *Angew. Chem.* **2018**, *130*, 16398−16402.
(34) Liu, J.; He, T.; Wang, Q.; Zhou, Z.; Zhang, Y.; Wu, H.; Li, Q.; Zheng, J.; Sun, Z.; Lei, Y.; Ma, J.; Zhang, Y. Confining Ultrasmall Bimetallic Alloys in Porous N−carbon for Use as Scalable and Sustainable Electrocatalysts for Rechargeable Zn−Air Batteries. *J. Mater. Chem. A* **2019**, *7*, 12451−12456.
(35) Fei, H.; Dong, J.; Feng, Y.; Allen, C. S.; Wan, C.; Volosskiy, B.; Li, M.; Zhao, Z.; Wang, Y.; Sun, H.; An, P.; Chen, W.; Guo, Z.; Lee, C.; Chen, D.; Shakir, I.; Liu, M.; Hu, T.; Li, Y.; Kirkland, A. I.; Duan, X.; Huang, Y. General Synthesis and Definitive Structural Identification of MN4C4 Single-Atom Catalysts with Tunable Electrocatalytic Activities. *Nat. Catal.* **2018**, *1*, 63−72.
(36) Fei, H.; Dong, J.; Arellano-Jiménez, M. J.; Ye, G.; Dong Kim, N.; Samuel, E. L. G.; Peng, Z.; Zhu, Z.; Qin, F.; Bao, J.; Yacaman, M. J.; Ajayan, P. M.; Chen, D.; Tour, J. M. Atomic Cobalt on Nitrogen-Doped Graphene for Hydrogen Generation. *Nat. Commun.* **2015**, *6*, 8668−8676.
(37) Yin, P.; Yao, T.; Wu, Y.; Zheng, L.; Lin, Y.; Liu, W.; Ju, H.; Zhu, J.; Hong, X.; Deng, Z.; Zhou, G.; Wei, S.; Li, Y. Single Cobalt Atoms with Precise N-Coordination as Superior Oxygen Reduction Reaction Catalysts. *Angew. Chem., Int. Ed.* **2016**, *55*, 10800−10805.
(38) Lv, J.; Rong, Z.; Sun, L.; Liu, C.; Lu, A.-H.; Wang, Y.; Qu, J. Catalytic conversion of biomass-derived levulinic acid into alcohols over nanoporous Ru catalyst. *Catal. Sci. Technol.* **2018**, *8*, 975−979.
(39) Jung, C. Y.; Zhao, T. S.; Zeng, L.; Tan, P. Vertically Aligned Carbon Nanotube-Ruthenium Dioxide Core-Shell Cathode for Non-Aqueous Lithium-Oxygen Batteries. *J. Power Sources* **2016**, *331*, 82−90.
(40) Ma, J.; Wang, X.; He, T.; Tan, M.; Zheng, J.; Wu, H.; Yuan, M.; Shen, R.; Zhang, Y.; Xiang, J. In situ Hybridization of CoOx Nanoparticles on N-doped Graphene through One Step Mineralization of Co-Responsive Hydrogels. *Dalton Trans.* **2017**, *46*, 6163−6167.
(41) Wohlgemuth, S.-A.; White, R. J.; Willinger, M.-G.; Titirici, M.-M.; Antonietti, M. A One-Pot Hydrothermal Synthesis of Sulfur and Nitrogen Doped Carbon Aerogels with Enhanced Electrocatalytic Activity in the Oxygen Reduction Reaction. *Green Chem.* **2012**, *14*, 1515−1523.
(42) Zhu, C.; Shi, Q.; Feng, S.; Du, D.; Lin, Y. Single-Atom Catalysts for Electrochemical Water Splitting. *ACS Energy Lett.* **2018**, *3*, 1713−1721.
(43) Yao, Y.; Hu, S.; Chen, W.; Huang, Z.-Q.; Wei, W.; Yao, T.; Liu, R.; Zang, K.; Wang, X.; Wu, G.; Yuan, W.; Yuan, T.; Zhu, B.; Liu, W.; Li, Z.; He, D.; Xue, Z.; Wang, Y.; Zheng, X.; Dong, J.; Chang, C.-R.; Chen, Y.; Hong, X.; Luo, J.; Wei, S.; Li, W.-X.; Strasser, P.; Wu, Y.; Li, Y. Engineering the Electronic Structure of Single Atom Ru Sites via Compressive Strain Boosts Acidic Water Oxidation Electrocatalysis. *Nat. Catal.* **2019**, *2*, 304−313.
(44) Zhang, S.; Lv, F.; Zhang, X.; Zhang, Y.; Zhu, H.; Xing, H.; Mu, Z.; Li, J.; Guo, S.; Wang, E. Ni@RuM (M=Ni or Co) Core@Shell Nanocrystals with High Mass Activity for Overall Water-Splitting Catalysis. *Sci. China Mater.* **2019**, *62*, 1868−1876.
(45) Zhou, W.; Jia, J.; Lu, J.; Yang, L.; Hou, D.; Li, G.; Chen, S. Recent Developments of Carbon-Based Electrocatalysts for Hydrogen Evolution Reaction. *Nano Energy* **2016**, *28*, 29−43.
(46) Xu, Y.; Tu, W.; Zhang, B.; Yin, S.; Huang, Y.; Kraft, M.; Xu, R. Nickel Nanoparticles Encapsulated in Few-Layer Nitrogen-Doped Graphene Derived from Metal−Organic Frameworks as Efficient Bifunctional Electrocatalysts for Overall Water Splitting. *Adv. Mater.* **2017**, *29*, 1605957.
(47) Du, B.; Meng, Q.-T.; Sha, J.-Q.; Li, J.-S. Facile Synthesis of FeCo Alloys Encapsulated in Nitrogen-Doped Graphite/Carbon Nanotube Hybrids: Efficient Bi-Functional Electrocatalysts for Oxygen and Hydrogen Evolution Reactions. *New J. Chem.* **2018**, *42*, 3409−3414.

DOI: 10.1021/acsami.9b17056
ACS Appl. Mater. Interfaces 2019, 11, 46912−46919

(48) Gao, W.-K.; Yang, M.; Chi, J.-Q.; Zhang, X.-Y.; Xie, J.-Y.; Guo, B.-Y.; Wang, L.; Chai, Y.-M.; Dong, B. In situ Construction of Surface Defects of Carbon-Doped Ternary Cobalt-Nickel-Iron Phosphide Nanocubes for Efficient Overall Water Splitting. *Sci. China Mater.* **2019**, *62*, 1285−1296.
(49) Hu, Q.; Li, G.; Li, G.; Liu, X.; Zhu, B.; Chai, X.; Zhang, Q.; Liu, J.; He, C. Trifunctional Electrocatalysis on Dual-Doped Graphene Nanorings−Integrated Boxes for Efficient Water Splitting and Zn−Air Batteries. *Adv. Energy Mater.* **2019**, *9*, 1803867.
(50) He, T.; Li, Z.; Sun, Z.; Chen, S.; Shen, R.; Yi, L.; Deng, L.; Yang, M.; Liu, H.; Zhang, Y. From Supramolecular Hydrogels to Functional Aerogels: A Facile Strategy to Fabricate Fe_3O_4/N-Doped Graphene Composites. *RSC Adv.* **2015**, *5*, 77296−77302.
(51) Hummers, W. S.; Offeman, R. E. Preparation of Graphitic Oxide. *J. Am. Chem. Soc.* **1958**, *80*, 1339.

DOI: 10.1021/acsami.9b17056
ACS Appl. Mater. Interfaces 2019, 11, 46912−46919